International Journal of Nanoelectronics and Materials
IJNeaM
ISSN 1985-5761 | E-ISSN 2232-1535

Effect of magnetic field on the structural, optical, and electrical properties of CdS nanoparticles in distilled water by using pulsed laser ablation

Yamamah K. Abdalaah[a*], Olfat A. Mahmood[a], Suaad S. Shaker[b]

[a] *University of Diyala, College of Science, Department of Physics, Diyala, Iraq*
[b] *University of Technology, Department of Applied Science, Baghdad, Iraq*
** Corresponding author. Tel.: +964-07710249221; e-mail: yamamahkhaled89@gmail.com*

Received 11 March 2024, Revised 14 June 2024, Accepted 11 July 2024

ABSTRACT

In this study, we investigated the impact that the incorporation of a magnetic field has on the properties of cadmium sulfide CdS nanoparticles as well as the performance of an n-CdS/p-Si heterojunction photodetector that was developed by the use of the pulsed laser ablation in a liquid method. Nd:YAG laser pulses (1.064 μm, 550 mJ) were utilized to ablate cadmium sulfide CdS nanoparticles in water. The synthesized nanoparticles were shown to have a polycrystalline hexagonal structure, as evidenced by the findings of the X-ray diffraction experiment, the crystallite size for cadmium sulfide CdS decreased from 4.611 nm to 4.518 nm. The lattice constants of cadmium sulfide CdS nanostructures were determined to be a = 4.1302, c = 6.702, and c/a=1.622. The strain and dislocation density of cadmium sulfide CdS exhibited an increase. Images taken from a field emission scanning electron microscope demonstrated the formation of spherical nanoparticles on the surface. A magnetic field was applied, increasing the CdS film's crystallinity. As a consequence of this enhancement, the particle size of the CdS decreased from 25.18 nm to 12.17 nm. A comparison was made between this and the size of the crystallites that appeared when no magnetic field was present. The EDS spectrum of magnetically prepared cadmium sulfide CdS films indicates the presence of Cd and S, and the weight percentage ratios [Cd]/[S], increase from 3.72 to 3.80. The transmission electron microscopy (TEM) pictures of CdS samples that were generated using a magnetic field contained particles of small size with a mean of 10.10 nanometers. From the FT-IR spectra of cadmium sulfide CdS prepared using a magnetic field within 400–4000 cm−1, the peaks (bands) of cadmium sulfide CdS at 617 cm^{-1} represent the bending vibration of Cd-S. As a result of the influence of a magnetic field, the optical energy gap of CdS nanoparticles increased from 2.30 eV to 2.72 eV, as indicated by the UV-Vis study. From PL emission spectra the values of the energy band gap of cadmium sulfide CdS increased from 2.45 eV at 505.7 to 2.47 eV when a magnetic field was applied. CdS NP films produced under the influence of a magnetic field were identified as having n-type characteristics by Hall effect assessments, Particle mobility was influenced by particle size. The effect of applying a magnetic field on the efficiency of the n-CdS/p-Si photodetector was investigated and analyzed. When a magnetic field was applied during ablation, the responsivity of n-CdS/p-Si heterojunction photodetectors increased from 0.498 A/W to 0.830 A/W at 510 nm. This was the result of the application of the magnetic field.

Keywords: *CdS, PLAL, Photodetector*

1. INTRODUCTION

Cadmium sulfide (CdS) is one of the most desirable types II and VI semiconductors because of its direct and wide (2.42 eV) band gap at room temperature[1, 2]. CdS is a stable substance that enables visible emission with optical absorption at 515 nm. Huggins compared the distribution of electrons in the valance band of CdS and diamond when he began researching CdS in 1925. In 1947, the French synthesized CdS from Cd vapor and H_2S and referred to it as incomplete phosphorus due to its lack of phosphorescence but strong photoconductivity[3]. CdS has two types of crystal structure, namely, wurtzite and zinc blend; wurtzite is the most stable and simplest phase to synthesize and is observed in bulk and nanostructures. By contrast, zinc alloy is utilized[4, 5]. CdS is not soluble in water but can be converted into soluble forms in dilute mineral acids. CdS demonstrates inherent n-type conductivity due to its significant band gap, which is crucial in various fields such as photonics, photoelectronics, photovoltaics, and photocatalysis [4].

Nano CdS exhibits distinct physical, chemical, and structural characteristics in comparison to its bulk form [4, 6]. There are a number of different processes that can be utilised in order to produce nano-CdS. These include chemical colloidal, sol-gel, hydrothermal, micro-emulsion, and solvothermal techniques [3]. Among II–VI compounds, CdS is a viable candidate for visible radiation detection[2]. Nano CdS has the ability to be shaped into a wide variety of shapes, including crystals, spheres, nanowires, dendrites, and sea urchin like.

Pulsed laser ablation in liquids (PLAL) is the most recently developed method for producing nanoparticles (NPs) and has received considerable attention as an innovative

technique[7]. PLAL is a physical method for the synthesis of NPs and does not involve any chemical reactions. It is environmentally friendly because of the lack of hazardous or toxic gases emitted[7]. This technique produces NPs in the form of a colloidal suspension and is safer than dry processing[7, 8]. Various parameters, including laser wavelength, laser energy, number of laser pulses, type of colloid solution, and pulse duration, can affect the characteristics of NPs synthesized using this method. This paper describes the synthesis of CdS NPs by ablation of a CdS target in distilled water with an Nd:YAG laser. The effect of magnetic field on the properties of NPs was determined and compared with published results.

2. EXPERTIMENTAL PART

CdS NP suspension was prepared by PLAL of CdS pellets at the bottom of a glass vessel with 2 mL of distilled water (DW) above the solid target. The target was created using 99.99% high-purity powder cadmium sulfide from Sigma–Aldrich with high-purity CdS. The distance between the solid target and the laser lens was 10 cm. A Q-switched Nd:YAG laser with a laser wavelength of 1064 nm was used to prepare colloidal CdS NPs at 300 pulses, 550 mJ laser energy, a laser frequency of 1 Hz, and with or without an external magnetic field by using four small external neodymium magnets of around 19 mT during laser ablation. The setup is shown in Figure (1). This was accomplished by positioning four magnets around the ablation vessel in such a way that the magnetic field was oriented at a right angle to the laser beam that was coming in. A Gauss and Tesla metre, more precisely the NVIS 621, was utilised in order to take the readings of the magnetic field. When it came to laser ablation with the assistance of a magnetic field, identical conditions were employed. The absorption spectra of the CdS NP solution were analyzed in the spectral region of (190–1100) nm under various conditions by using a spectrophotometer (model-Shimadzu, 1800) with a double beam of UV-vis at room temperature [9-11]. The solutions were placed in quartz cells (1 cm optical path). The optical properties of CdS NP colloids were determined. Wavelength absorbance output data were analyzed using OriginLab 8.5 to determine the optical energy band gap and absorption coefficient. A PL spectrophotometer (ELICO, SL174, Xe lamp as power supply) was utilized to investigate photoluminescence, which is a physical phenomenon used to examine the electronic structure of matter. External energy was utilized to stimulate electrozz. PL data were used to evaluate importation characteristics, including the determination of band gap. In PL measurements, the wavelength range was approximately 200–900 nm. The structure and crystallinity of NPs were analyzed using an X-ray diffractometer (XRD, SHIMADZU, 6000). A field emission scanning electron microscope (FE-SEM, MIRA3 model-TESCAN) was used to investigate the structure of NPs. Transmission electron microscopy (TEM) was used to measure the size, shape, and type of CdS assemblies. FTIR (IRAFFINITY-1) was used to determine the type of bonds between the resultant compound (CdS) within 400–4000 cm−1) by evaluating the groups and bands in the infrared spectrum. A highly reflective p-type silicon substrate orientated along the (111) plane, measuring 1 cm^2 in area, and possessing an electrical resistance of 3–5 Ω.cm was utilized as the base for constructing the photodetector. After a washing procedure, the silicon substrates were etched with diluted HF to eliminate any natural oxide present on the surface. Following this, the substrates were rinsed for 15 minutes with distilled water in an ultrasonic chamber (Cerry PUL 125). At ambient temperature, a CdS NP colloid measuring 0.8 µm in thickness was applied to the silicon substrate via a Holmarc HO-TH-05 spin coater. By employing thermal resistance, In and Al films were deposited onto the rear side of the silicon substrate and the nanostructured CdS NP colloid film to establish ohmic contacts (Fig. 1(b)). Electrodes and external devices were connected with silver paste. The current-voltage properties of the CdS NP colloid heterojunction were investigated under illumination and without light at room temperature. Figure 2 shows the experimental setup used to measure photodetector responsivity.

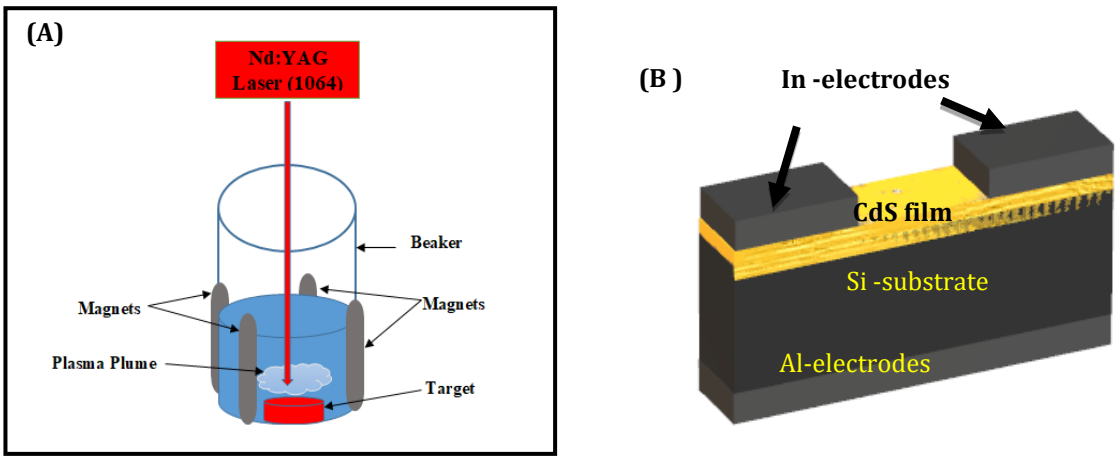

Figure 1. (a) Schematic of pulsed laser ablation with magnetic field assistance. (b) Cross section of CdS/Si film photodetector

3. RESULTS AND DISCUSSION

3.1. Structure Properties

The XRD analysis in Figure 2 for CdS NPs prepared with and without a magnetic field revealed that CdS has a polycrystalline hexagonal structure according to JCPDS card (no:41-1049) with different orientations (002), (110), and (112) and a preferred orientation in the (002) direction with 2θ = 26.5783°, 43.8014°, and 51.9674° [12, 13]. From 2θ = 26.5783° and 43.8014°, the lattice constants of CdS nanostructures were determined to be a = 4.1302, c = 6.702, and c/a=1.622. These results correspond to those reported in the literature[14-16]. Several factors influence the FWHM of XRD data, including crystal quality, grain size, and inhomogeneous stress distribution. In comparison with the XRD pattern without a magnetic field, it was observed in the XRD pattern of CdS nanoparticles that were synthesised with a magnetic field that the strength of the CdS peak significantly increased. This conclusion can be attributed to the elevation in growth and nucleation qualities that occurred as a result of the low diffusion mobility of deposited atoms and the increase in crystallinity of the film material, which ultimately led to an improvement in the crystalline structure [17]. The average crystallite size (D_{av}) can be calculated using the Debye–Scherrer's formula[18].

$$D_{av} = K\lambda / \beta \cos\theta \quad (1)$$

K represents a constant determined by the material's form, ranging between 0.9 and 1; β: is the full-width at half maximum in radians; θ is the angle of Bragg diffraction; and λ is the wavelength of the X-rays that hit the target.

The crystallite size for CdS decreased from 4.611 nm to 4.518 nm due to the improvement in the crystallinity of the CdS film applied with a magnetic field compared with the crystallite size without a magnetic field. Dislocation density and strain for CdS NPs generated on the film were calculated using the following equations:

$$\delta = 1/ (D^2_{av}) \quad (2)$$

$$\varepsilon = (\beta \cos \theta) / 4 \quad (3)$$

where δ represents the dislocation density, and ε represents the strain.

Under the influence of a magnetic field, the strain and dislocation density of CdS exhibited an increase as shown in Table 1. Applying a magnetic field while using a laser caused the plasma to be contained and led to a higher degree of particle fragmentation. [19].

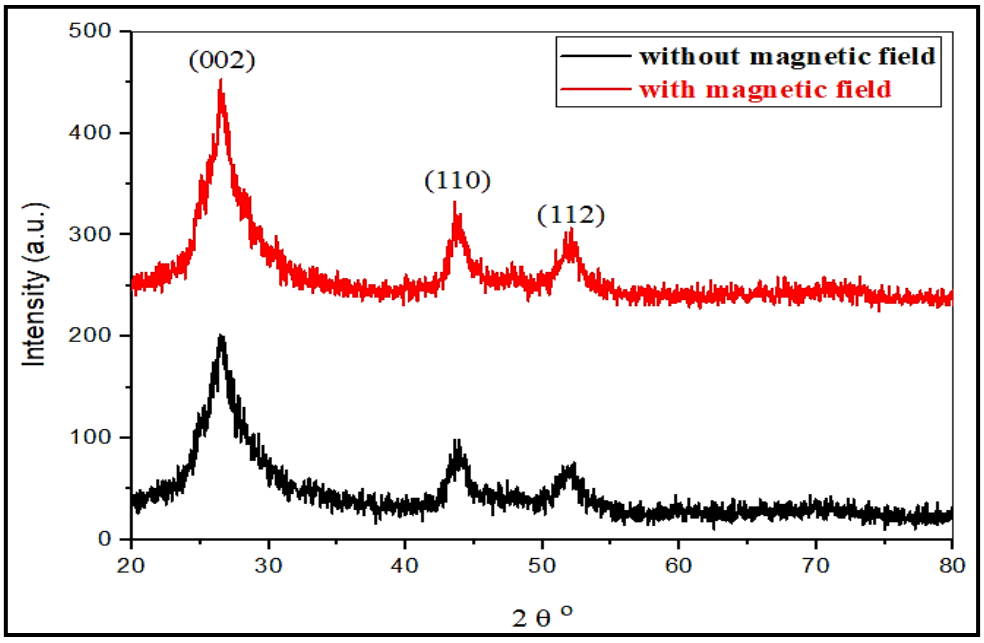

Figure 2. XRD patterns of CdS NPs synthesised with and without magnetic field

Table 1. Dislocation density and strain of CdS NPs with and without magnetic field.

CdS	(δ) Dislocation density nm^{-2}	(ε) Strain (unit-free)
Without magnetic field	$10.9295*10^{-2}$	$6.5692*10^{-1}$
With magnetic field	$11.094*10^{-2}$	$6.6185*10^{-1}$

The FESEM images of the CdS thin films that were made by laser ablation in a magnetic field (B=0 and B=19 mT) are shown in Figure 3. The CdS that is made without a magnetic field is spherical and has an average size of 25.18 nm. Some of the CdS particles are NPs that have clumped together to make big particles (Fig. 3(a)). If you took away the magnetic field, the film morphology was less even, less thick, and less packed together. When a magnetic field was applied, the CdS film became more crystallised. This caused the crystallites to get smaller, from 25.18 nm to 12.17 nm. The difference was measured against the size of the crystallites when a magnetic field wasn't present. The plasma plume was contained by a magnetic field that was made when four magnets used for the same reason were put together. It looks like this result and the XRD data are linked. The XRD data agrees with this outcome. This result is consistent with the XRD data.

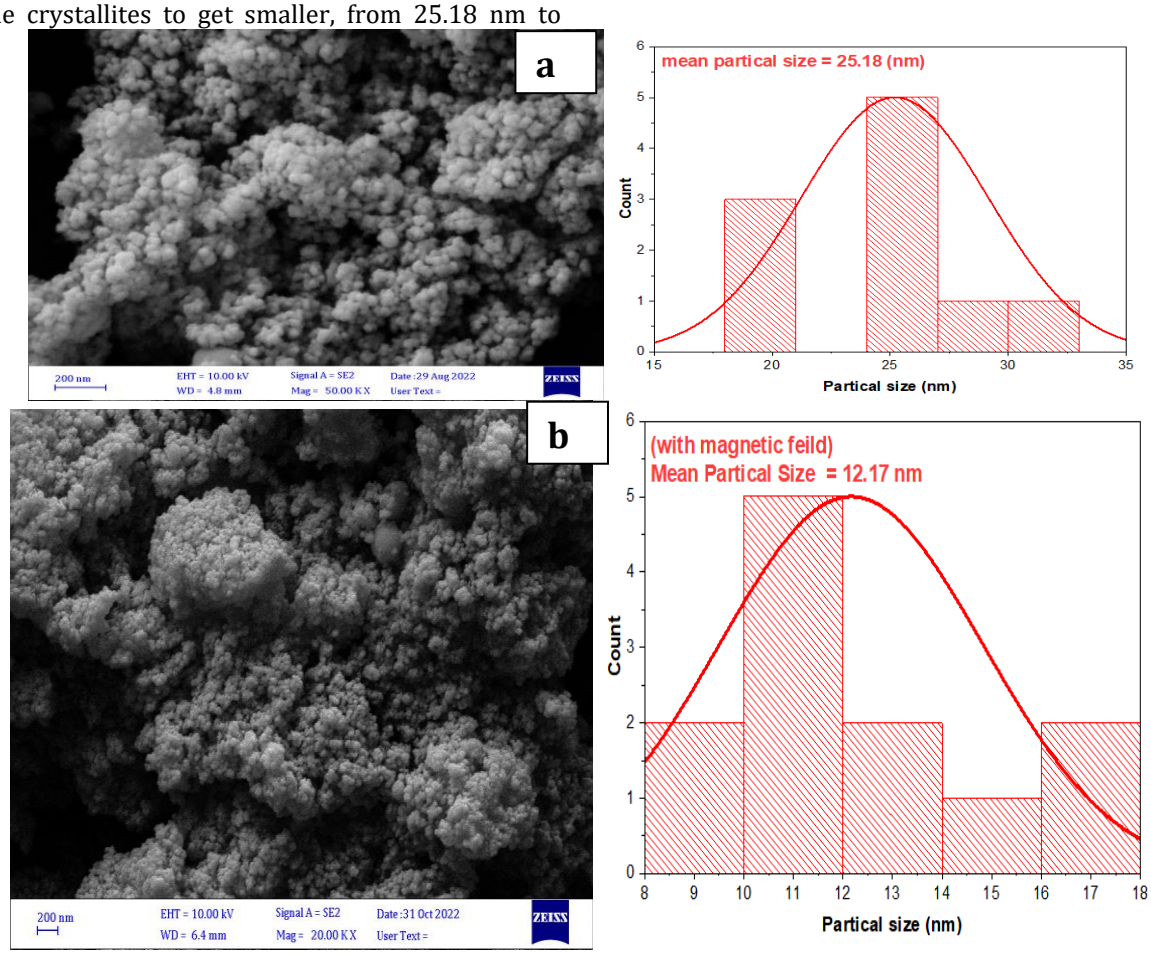

Figure 3. FESEM images of CdS NPs synthesized: (a) without a magnetic field, (b) with a magnetic field

The EDS spectrum of magnetically prepared CdS films is shown in Figure 4. The spectra indicate the presence of Cd and S as well as peaks related to the glass substrate, including O, C, S, Si, and Na. The lack of magnetic peaks indicates that the position of the magnet has no effect on the laser plume. The weight percentage ratios [Cd]/[S], as determined by EDS analysis, for CdS NPs with and without a magnetic field are 3.72 and 3.80, respectively. The increase in the relative weight ratio of cadmium and sulfur in CdS films could be attributed to the magnetic field's effect on nanoatom deposition and film formation. Exposure to a magnetic field can cause a change in the arrangement and distribution of atoms in films, altering the ratio of their constituent chemical constituents. For example, the magnetic effect may cause a change in atoms' chemical transitions during film growth, resulting in a minor alteration in the final film composition [18].

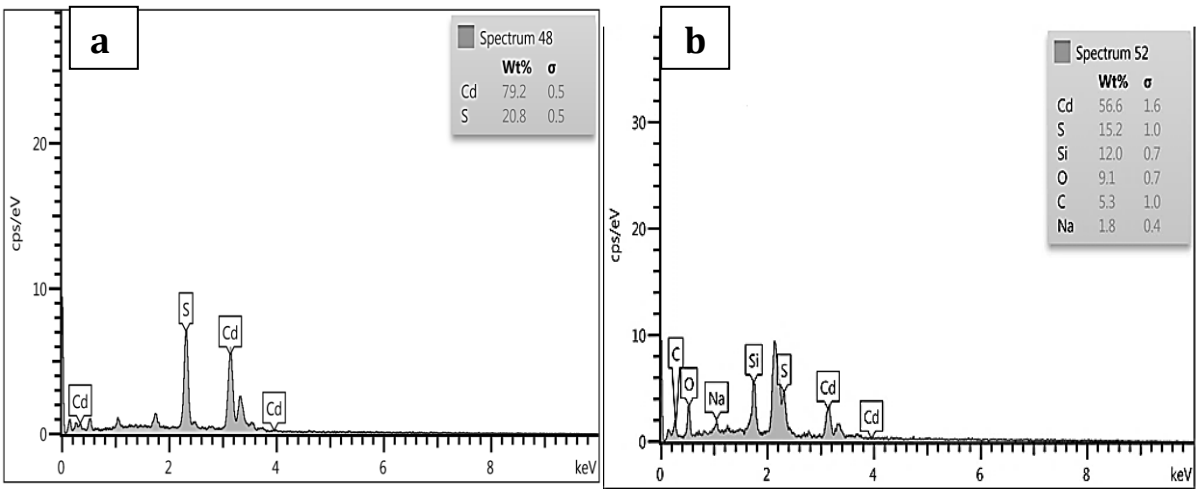

Figure 4. EDX spectra for CdS NPs synthesized (a) without a magnetic field and (b) with a magnetic field

A comparison of the particle size distribution of CdS nanoparticles that were synthesised with and without the use of a magnetic field is shown in Figure 5. The transmission electron microscopy (TEM) pictures of CdS samples that were processed without the use of a magnetic field revealed the production of aggregated spherical and elongated nanoparticles (NPs), as shown in Figure (5a). CdS has an average size of 12.56 nanometers, as indicated by the particle size distribution and its measurements. According to the illustration in Figure (5b), the CdS sample that was generated using a magnetic field contained particles of a small size. The fragmentation of CdS nanoparticles was sped up by the application of an external magnetic field, which led to a particle size distribution with a mean of 10.10 nanometers. The application of the magnetic field resulted in an increase in the temperature of the plasma, but the size of the cluster also decreased [19]. This result is consistent with the data obtained from XRD and FESEM.

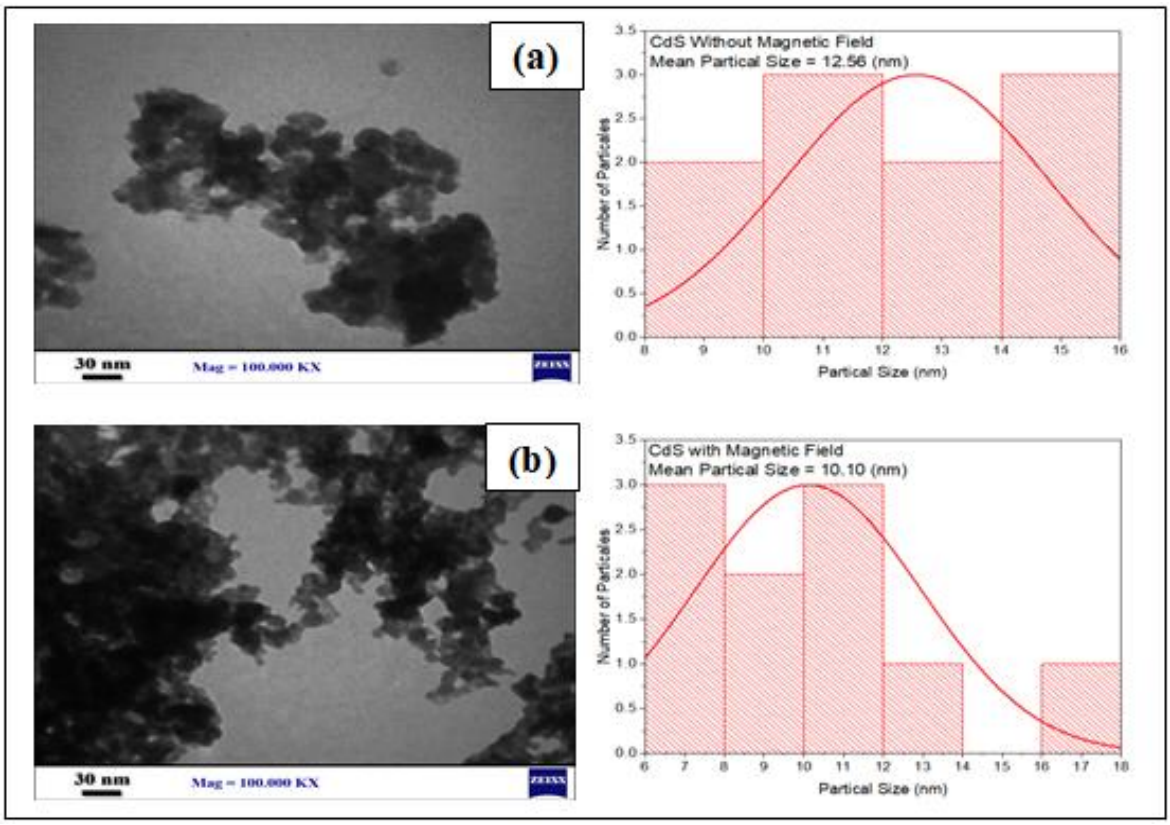

Figure 5. TEM images and size distribution histograms of CdS colloidal NPs prepared a) without a magnetic field and b) with a magnetic field.

Figure 6 displays the FT-IR spectra of CdS prepared using a magnetic field within 400–4000 cm^{-1}. As shown in Figure (6), the peaks (bands) of CdS at 617, 1111, 1620, 2924, and 3433 cm^{-1} represent the bending vibration of Cd-S, C-O, O-H, C=O, O-H, and O-H/N-H, respectively. Because of the moisture content in CdS nanoparticles, vibrations

associated with the O-H out of plane bending vibration of H_2O molecules have been detected. The presence of respective absorption peaks and bands in the FT-IR spectrum confirms the presence of CdS molecules, impurity traces caused by the chemical reaction of the various precursors utilized, and water molecules or hydroxide ions in the produced nanoparticles [20]. When a magnetic field is present, the absorption band intensity decreases and the FT-IR spectra shift slightly to higher wavenumbers. Changes in FT-IR spectra can represent the effect of a magnetic field on the arrangement of molecules or atoms in samples, influencing their interaction with the optical radiation utilized in FT-IR analysis and resulting in changes in the material's optical and chemical properties [20].

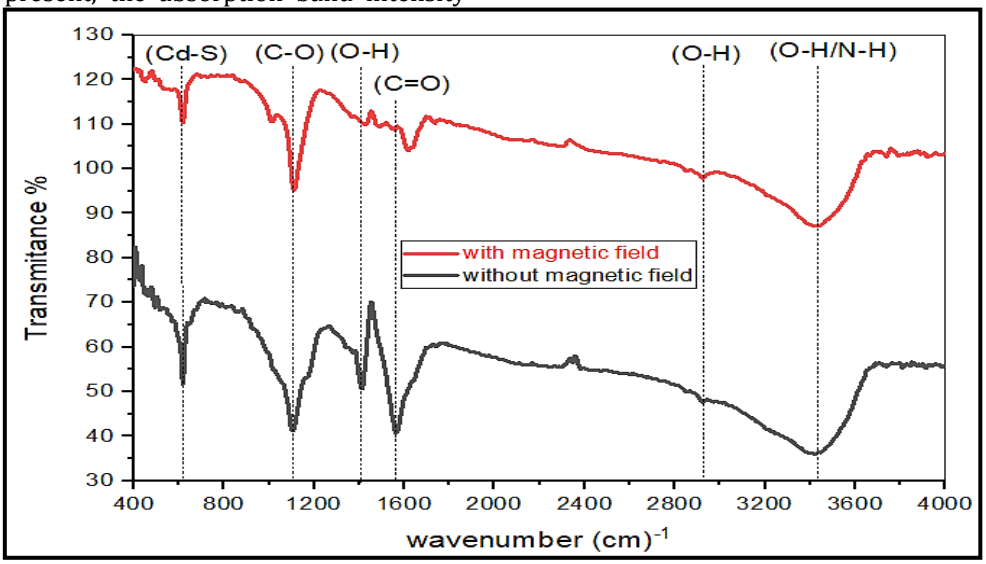

Figure 6. FT-IR spectra of CdS NPs synthesized with and without a magnetic field

3.2. Optical Properties

The optical absorption of colloidal CdS NP solution prepared with and without a magnetic field is illustrated in Figure 7. The results indicated that the light absorption of cadmium sulfide nanoparticles manufactured in the presence of a magnetic field was much higher than that of those manufactured without the presence of a magnetic field. Whether samples were treated with or without a magnetic field, the quantum size effect (QSE) was found to be responsible for the detection of an absorption peak at a wavelength of 500 nm. The application of a magnetic field resulted in a decrease in the size of CdS nanoparticles (NPs) and an increase in the concentration of NPs. This discovery is interesting because it shows that optical properties can be changed by applying a magnetic field to the material. The presence of an external magnetic field increased the plasma lifetime and density [21, 22]. By using the Tauc relationship, we were able to confirm the energy gap, for example, of CdS NPs with and without the presence of a magnetic field [20, 21]. Through the utilization of Tauc's relationship, we were able to ascertain the energy gap Eg of CdS NPs with and without the presence of a magnetic field [23].

$$\alpha h\nu = A(h\nu - Eg)^{1/2} \quad (4)$$

A is a constant, while hν represents the energy of a photon. The energy gap was determined by plotting (ahν)2 against (hν) and identifying the intercept of the straight line with the hν axis as the band gap[24, 25].

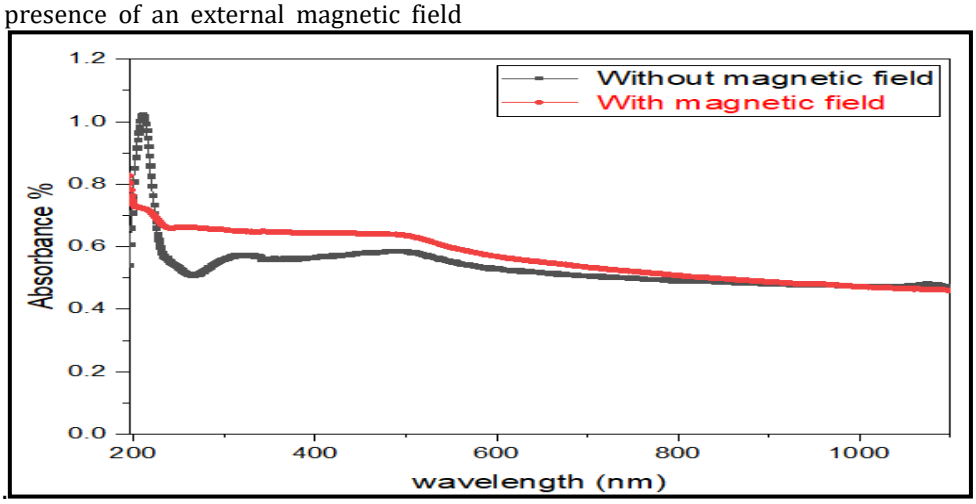

Figure 7. Absorbance versus wavelength of CdS NPs prepared with and without a magnetic field

The energy gap is depicted in Figure 8. The transition between CdS NPs is direct [26]. The optical energy gap for CdS NPs increased from 2.30 eV to 2.72 eV when a magnetic field was applied because of the increase in NP concentration and the decrease in the particle size of CdS.

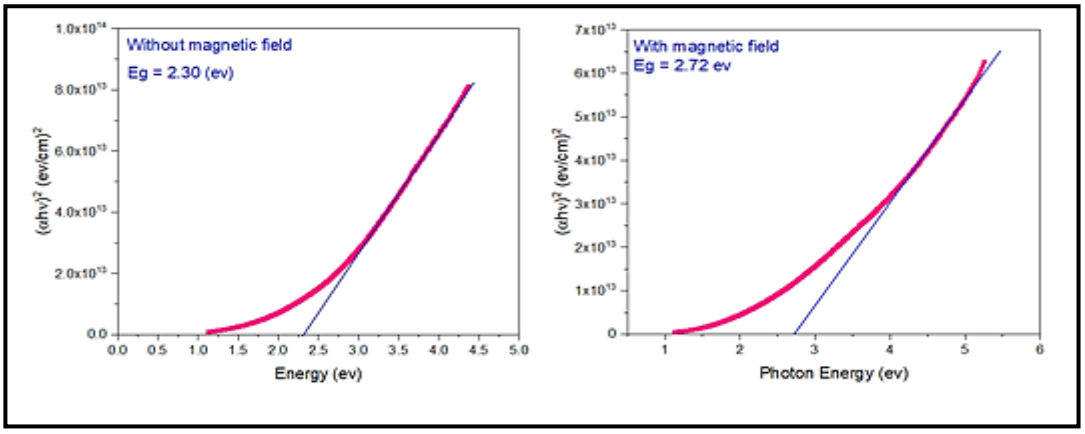

Figure 8. Direct optical energy gap for CdS NPs prepared with and without a magnetic field.

Figure 9 illustrates the PL emission spectra of CdS NPs prepared with and without a magnetic field. The PL spectra show a peak located at 501.094 nm, corresponding to 2.47 eV. The PL emission of the CdS sample prepared with a magnetic field has a single identifiable emission peak and a high intensity with a narrow FWHM. The values of the energy band gap of CdS increased from 2.45 eV at 505.7 to 2.47 eV when a magnetic field was applied, corresponding to optical absorption measurements. This change in the band gap implies that the magnetic field modifies the electronic makeup of CdS NPs, influencing their optical characteristics [27]. Magnetic fields can improve the mobility of charge carriers (electrons and holes) within CdS nanoparticles. This improved mobility may result in more effective radiative recombination processes and higher-intensity photoluminescence emission [27].

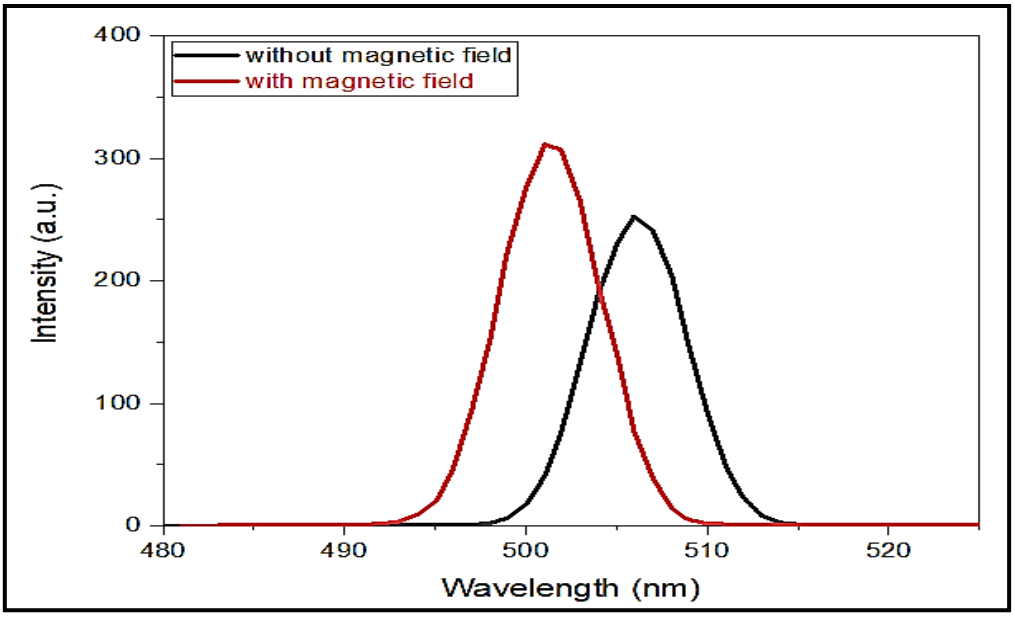

Figure 9. PL spectra of CdS NP colloid synthesized with and without a magnetic field

3.3. Electrical Properties

CdS NP films produced under the influence of a magnetic field were identified as having n-type characteristics by Hall effect assessments. Table 2 shows the electrical mobility and resistivity of CdS produced with the application of a magnetic field. Particle mobility was influenced by particle size, with the mobility of CdS nanoparticles decreasing in the presence of a magnetic field. A magnetic field can align CdS NPs along the field lines or lead them to form aggregates, limiting their movement and decreasing their mobility [28]. The magnetic field can introduce additional scattering mechanisms for charge carriers within CdS NPs, leading to a decrease in their mobility. These scattering mechanisms include interactions with magnetic field-induced defects or changes in scattering caused by the field. Despite the decrease in electrical mobility, the electrical resistivity of CdS NPs decreases in the presence of a magnetic field. The decrease in resistivity can be influenced by factors, such as

changes in carrier concentration, carrier scattering mechanisms, or changes in conductivity because of magnetic field effects[28].

Table 2. Electrical mobility and resistivity of CdS NPs synthesized with a magnetic field

CdS	Electrical Mobility ($cm^2 V^{-1} s^{-1}$) * 10^3	Electrical Resistivity (Ω cm)
Without magnetic field	2.83	5.28
With magnetic field	0.0843	9.177 *10^{-2}

As depicted in Figure 10, the dark I-V characteristics of n-CdS/p-Si heterojunction were measured over the voltage range of – 7.5 V to + 7.5 V by applying a magnetic field. The heterojunction exhibited rectification properties, which were enhanced by the application of a magnetic field by increasing the charge transfer and decreasing the resistivity[29, 30]. The dark forward current increased from 490 µA to 600 µA, and the reverse current increased from 15.4 µA to µ10.5A, as illustrated in Figure 10. The rectification factor decreased from 31.818 to 57.142. This improvement is attributed to an improvement in junction properties (a reduction in structural defects and surface states).

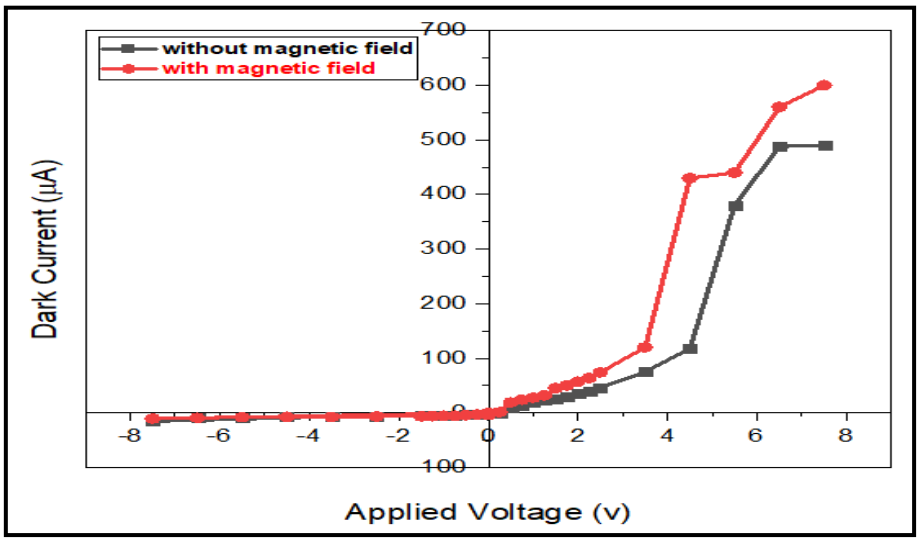

Figure 10. Dark I-V characteristic of n-CdS/p-Si heterojunction prepared with and without a magnetic field under forward and reverse bias

Figure 11 shows the I-V characteristics of the n-CdS/p-Si heterojunction under white light of different intensities and a magnetic field. The creation of electron-hole pairs enhanced the current of the photodetector when exposed to light. As the light intensity grew, the photocurrent rose due to the growing number of photogenerated electron-hole pairs [31]. As illustrated in Figure 11, the photocurrent of the magnetically field-made photodetector was greater than that of the non-magnetically field-made photodetector. The substantial surface area and light-absorbing capacity may be the cause of the rise in photocurrent that occurs after the introduction of a magnetic field. When a 7.5 V bias magnetic field was introduced, the photodetector exhibited an on/off ratio of 371.428, calculated as the ratio of photocurrent to dark current (Iph/Id). Enhancing the photodetector's photosensitivity was achieved by utilising a magnetic field, leading to an increase in the sensitive region and a decrease in particle size[31].

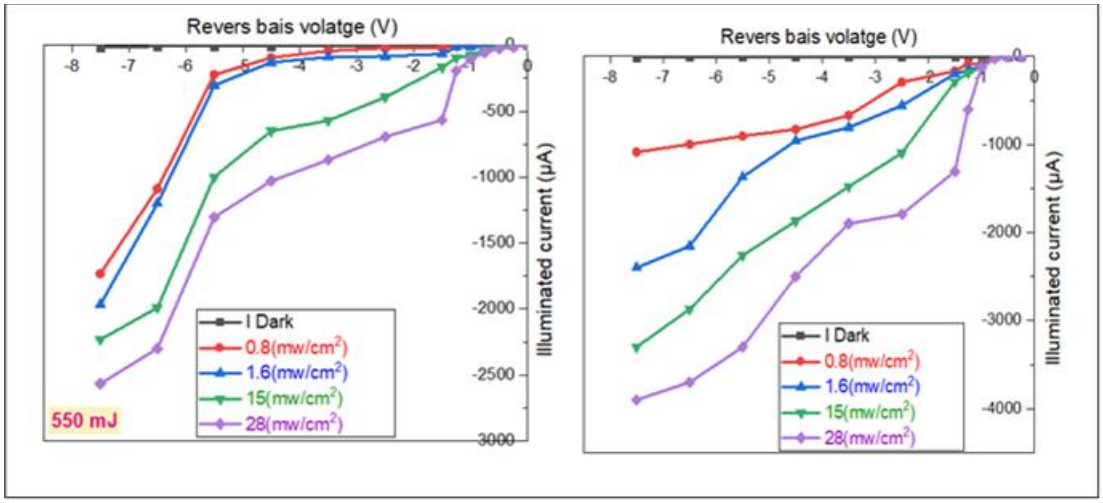

Figure 11. Dark and illuminated (I-V) characteristic of n-CdS/p-Si HJ photodetectors synthesized (a) with a magnetic field and (b) without a magnetic field

The spectral responsivity of n-CdS/p-Si heterojunction was measured within the wavelength range of 360–910 nm with a bias of 0.65 V and calculated with equation[33].

R_λ=(ph/in or V/in) (5)

where the photo current is denoted by ph, the voltage current is denoted by V, and the power under light is shown by in. In Figure 12, there is an illustration of the impact that the application of a magnetic field has on the spectrum responsivity of a nanostructured n-CdS/p-Si heterojunction photodetector.

There are three response peaks seen by the n-CdS/p-Si) photodetector. It is located at 411 nm and has a responsivity of 0.299 A/W. The initial peak is located at this wavelength. In terms of its responsivity, the second peak can be seen at 560 nm and has a value of 0.498 A/W. The absorption edge of the bulk silicon substrate is centred at 860 nm, which corresponds to the third peak that can be found at that wavelength [34]. Following the application of a magnetic field, it was determined that there were just two peaks. Both the first peak, which is located at 510 nm and has a rising responsivity of 0.830 A/W, and the second peak, which is located at 860 nm, are located there. The short-wavelength response was brought about by photon absorption in the CdS film, which was brought about by the shift of the depletion region towards the CdS which was brought about by the application of bias. Due to the significant amount of photon absorption that happened in the silicon substrate, the reaction that took place at NIR wavelengths took place. A blue shift, which is a widening of the energy gap, and the appearance of a shallow new energy level, which is the result of the division of CdS energy levels as a result of an external magnetic field, are the two factors that contribute to the formation of the peak at 510 nm [35]. It was possible to improve the separation of photogenerated carriers by applying a reverse bias to the photodetector, which resulted in an increase in detector sensitivity. Outside of the depletion region, carriers were manufactured, and the diffusion length was recombined; nevertheless, this did not contribute to the photocurrent accumulation [36, 37].

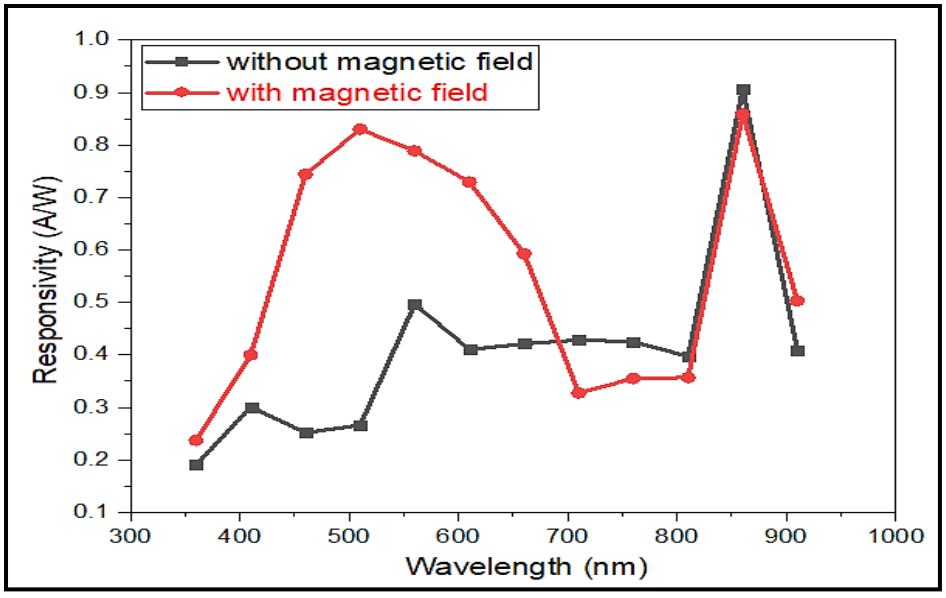

Figure 12. Spectral responsivity of n-CdS/p-Si photodetector synthesized by laser ablation with a magnetic field

4. CONCLUSION

Cadmium sulphide nanoparticles (CdS NPs) can be produced in distilled water using laser ablation with the assistance of a magnetic field. The X-ray diffraction pattern of CdS nanoparticles synthesised under the influence of a magnetic field exhibited heightened intensity in the CdS peak. Upon the application of a magnetic field, the particle size of CdS NPs reduced from 25.18 nm to 12.17 nm, as indicated by FESEM and XRD data. Applying a magnetic field raised the optical energy gap of CdS NPs from 2.30 eV to 2.72 eV. An investigation was conducted on how the magnetic field impacts the operation of the n-CdS/p-Si photodetector. The photodetector's performance was significantly enhanced upon exposure to a magnetic field. The responsivity at 510 nm rose from 0.498 A/W to 0.830 A/W.

REFERENCES

[1] A. El-Bially, R. Seoudi, W. Eisa, A. Shabaka, R. Abd El-Hamid, and R. Ramadan, "Preparation, characterization and physical properties of CdS nanoparticles with different sizes," *Journal of Applied Sciences Research,* vol. 8, no. 2, pp. 676-685, 2012.

[2] A. Dumbrava, C. Badea, G. Prodan, and V. Ciupina, "Synthesis and characterization of cadmium sulfide obtained at room temperature," *Chalcogenide Lett,* vol. 7, no. 2, pp. 111-118, 2010.

[3] N. Hullavarad, S. Hullavarad, and P. Karulkar, "Cadmium sulphide (CdS) nanotechnology: synthesis and applications," *Journal of nanoscience and nanotechnology,* vol. 8, no. 7, pp. 3272-3299, 2008.

[4] N. Qutub, "Cadmium sulphide nanoparticles," Ph. D. Thesis, 2013.

[5] K. P. Acharya, "Photocurrent spectroscopy of CdS/plastic, CdS/glass, and ZnTe/GaAs hetero-pairs formed with pulsed-laser deposition," Bowling Green State University, 2009.

[6] P. S. Chowdhury, P. Sen, and A. Patra, "Optical properties of CdS nanoparticles and the energy transfer from CdS nanoparticles to Rhodamine 6G," *Chemical Physics Letters,* vol. 413, no. 4-6, pp. 311-314, 2005.

[7] H. Zeng *et al.*, "Nanomaterials via laser ablation/irradiation in liquid: a review," *Advanced Functional Materials,* vol. 22, no. 7, pp. 1333-1353, 2012.

[8] N. Semaltianos, "Nanoparticles by laser ablation," *Critical reviews in solid state and materials sciences,* vol. 35, no. 2, pp. 105-124, 2010.

[9] Y. K. Abdalaah, O. A. Mahmood, S. S. Shaker, " Preparation of a nanostructured CdTe@CdS core-shell /Si photodetector by two-step laser ablation in liquid", Journal of Optics, vol. 0123456789, no. 1, 2024.

[10] S. S. Shaker, R. A. Ismail, D. S. Ahmed, "High-Responsivity Heterojunction Photodetector Based on Bi2O3-Decorated MWCNTs Nanostructure Grown on Silicon via Laser Ablation in Liquid", Journal of Inorganic and Organometallic Polymers and Materials, 32(5):1-8.

[11] R. A. Ismail, S. S. Shaker, A. M. Mousa,(2021). Study the optoelectronic properties of PbI2 nanorods/Si photodetector prepared by magnetic field-assisted laser deposition route. Optics & Laser Technology. 140, 107042.

[12] R. Elilarassi, S. Maheshwari, and G. Chandrasekaran, "Structural and optical characterization of CdS nanoparticles synthesized using a simple chemical reaction route," *Optoelectronics and Advanced Materials-Rapid Communications,* vol. 4, no. March 2010, pp. 309-312, 2010.

[13] M. Li, W. Ren, R. Wu, and M. Zhang, "CeO2 enhanced ethanol sensing performance in a CdS gas sensor," *Sensors,* vol. 17, no. 7, p. 1577, 2017.

[14] E. Vaghri and D. Dorranian, "Effect of ablation environment on the characteristics of graphene nanosheets produced by laser ablation," *Studia Universitatis Babes-Bolyai. Chemia,* vol. 61, no. 4, pp. 277-285, 2016.

[15] J. Chang and E. R. Waclawik, "Colloidal semiconductor nanocrystals: controlled synthesis and surface chemistry in organic media," *RSC Advances,* vol. 4, no. 45, pp. 23505-23527, 2014.

[16] B. Sharma and R. Purohit, *Semiconductor heterojunctions*. Elsevier, 2015.

[17] N. Wakiya, T. Kawaguchi, N. Sakamoto, H. Das, K. Shinozaki, and H. Suzuki, "Progress and impact of magnetic field application during pulsed laser deposition (PLD) on ceramic thin films," *Journal of the Ceramic Society of Japan,* vol. 125, no. 12, pp. 856-865, 2017.

[18] F. Ouachtari, A. Rmili, B. Elidrissi, A. Bouaoud, H. Erguig, and P. Elies, "Influence of bath temperature, deposition time and S/Cd ratio on the structure, surface morphology, chemical composition and optical properties of CdS thin films elaborated by chemical bath deposition," *Journal of modern physics,* vol. 2011, 2011.

[19] A. Serkov *et al.*, "Influence of external magnetic field on laser breakdown plasma in aqueous Au nanoparticles colloidal solutions," *arXiv preprint arXiv:1602.08335,* 2016.

[20] SURESH KUMAR, J.K. SHARMA, " Stable phase CdS nanoparticles for optoelectronics: A study on surface morphology, structural and optical characterization", Materials Science-Poland, 34(2), 2016, pp. 368-373.

[21] M. A. Valverde-Alva *et al.*, "Effect of the magnetic field on the synthesis of colloidal silver and gold nanoparticles by laser ablation in bidestilated water," *Momento,* no. 63, pp. 1-11, 2021.

[22] K. K. Kim, M. Roy, H. Kwon, J. K. Song, and S. M. Park, "Laser ablation dynamics in liquid phase: The effects of magnetic field and electrolyte," *Journal of Applied Physics,* vol. 117, no. 7, 2015.

[23] C. M. Wolfe, N. Holonyak, and G. E. Stillman, *Physical Properties of Semiconductors*. prentice Hall, 1989.

[24] R. A. Ismail, G. M. Sulaiman, M. H. Mohsin, and A. H. Saadoon, "Preparation of silver iodide nanoparticles using laser ablation in liquid for antibacterial applications," *IET nanobiotechnology,* vol. 12, no. 6, pp. 781-786, 2018.

[25] R. A. Ismail, "Improved characteristics of sprayed CdO films by rapid thermal annealing," *Journal of Materials Science: Materials in Electronics,* vol. 20, pp. 1219-1224, 2009.

[26] R. A. Ismail, O. A. Abdulrazaq, and K. Z. Yahya, "Preparation and characterization of In 2 O 3 thin films for optoelectronic applications," *Surface Review and Letters,* vol. 12, no. 04, pp. 515-518, 2005.

[27] Weiwei Gong, Zhuhong Zheng, Jinju Zheng, Wei Gao, Xuebing Hu and Xinguang Ren, " Luminescence Study of Water-Soluble CdS Nanoparticles Produced by Femtosecond Laser Ablation at High Laser Fluence", J. Phys. Chem. C 2008, 112, 9983–9987.

[28] Y.-H. Lin, "Structure and properties of transparent conductive ZnO films grown by pulsed laser deposition (PLD)," University of Birmingham, 2010.

[29] R. A. Ismail, K. I. Hassan, O. A. Abdulrazaq, and W. H. Abode, "Optoelectronic properties of CdTe/Si heterojunction prepared by pulsed Nd: YAG-laser deposition technique," *Materials science in semiconductor processing,* vol. 10, no. 1, pp. 19-23, 2007.

[30] E. T. Salim, R. A. Ismail, M. A. Fakhri, B. G. Rasheed, and Z. T. Salim, "Synthesis of cadmium oxide/Si heterostructure for two-band sensor application," *Iranian Journal of Science and Technology, Transactions A: Science,* vol. 43, no. 3, pp. 1337-1343, 2019.

[31] J. Yin *et al.*, "Engineered tunneling layer with enhanced impact ionization for detection improvement in graphene/silicon heterojunction photodetectors," *Light: Science & Applications,* vol. 10, no. 1, p. 113, 2021.

[32] R. A. Ismail, S. A. Zaidan, and R. M. Kadhim, "Preparation and characterization of aluminum oxide nanoparticles by laser ablation in liquid as passivating and anti-reflection coating for silicon photodiodes," *Applied Nanoscience,* vol. 7, pp. 477-487, 2017.

[33] J. D. Vincent, *Fundamentals of infrared detector operation and testing*. 1990.

[34] V. Dhyani and S. Das, "High-speed scalable silicon-MoS2 PN heterojunction photodetectors," *Scientific reports,* vol. 7, no. 1, p. 44243, 2017.

[35] H. Guo *et al.*, "High-speed and broadband spectral photodetectors based on β-In2Se3/Si heterojunction," *Materials Science in Semiconductor Processing,* vol. 138, p. 106304, 2022.

[36] A. M. El-Mahalawy and A. R. Wassel, "Enhancement of organic/inorganic hybrid photodetector based on pentacene/n-Si by surface plasmonic effect of gold and silver nanoparticles: A comparative study," *Optics & Laser Technology,* vol. 131, p. 106395, 2020.

[37] M. Tanabe, "Evaluation of the nonlinearity of silicon photodiodes for ultraviolet light detection," *Optics & Laser Technology,* vol. 138, p. 106852, 2021.